J|A|C|S
ARTICLES

Published on Web 03/31/2009

Magnetic Anisotropy of Dysprosium(III) in a Low-Symmetry Environment: A Theoretical and Experimental Investigation

Kevin Bernot,[†,‡] Javier Luzon,[†] Lapo Bogani,[†,§] Mael Etienne,[†,‡] Claudio Sangregorio,[†] Muralidharan Shanmugam,[†] Andrea Caneschi,[†] Roberta Sessoli,[*,†] and Dante Gatteschi[*,†]

Department of Chemistry, University of Florence, Via della Lastruccia 3, 50019 Sesto Fiorentino, Italy, Laboratory SCR/MI-INSA, INSA-Rennes, 20 av. des buttes de Coësmes, CS 14315, 35043 Rennes Cedex, France, and 1. Physikalisches Institut, Universität Stuttgart, Pfaffenwaldring 57, D-70550 Stuttgart, Germany

Received December 23, 2008; E-mail: dante.gatteschi@unifi.it

Abstract: A mixed theoretical and experimental approach was used to determine the local magnetic anisotropy of the dysprosium(III) ion in a low-symmetry environment. The susceptibility tensor of the monomeric species having the formula $[Dy(hfac)_3(NIT-C_6H_4-OEt)_2]$, which contains nitronyl nitroxide (NIT−R) radicals, was determined at various temperatures through angle-resolved magnetometry. These results are in agreement with ab initio calculations performed using the complete active space self-consistent field (CASSCF) method, validating the predictive power of this theoretical approach for complex systems containing rare-earth ions, even in low-symmetry environments. Susceptibility measurements performed with the applied field along the easy axis eventually permitted a detailed analysis of the temperature and field dependence of the magnetization, providing evidence that the Dy ion transmits an antiferromagnetic interaction between radicals but that the Dy−radical interaction is ferromagnetic.

Introduction

Magnetic anisotropy plays a crucial role in magnetic bistability and related memory effects, in both traditional magnets and low-dimensional molecular materials such as single-molecule magnets (SMMs)[1] and single-chain magnets (SCMs).[2] In the design of new SMMs and SCMs with increased blocking temperatures (T_B), good control of the magnetic exchange (J), and consequently of the spin ground state of SMMs, has been achieved, leading to a record spin value as high as $^{83}/_{2}$.[3] Much more remains to be done to also engineer the magnetic anisotropy, and in fact, the record T_B value of $Mn_{12}OAc$, the archetypal SMM, has only recently been broken.[4]

The magnetic anisotropy of an exchange-coupled system depends not only on the individual anisotropies of the metal ions but also on the relative orientation of the local axes. When the anisotropy is large, this may give rise to spin noncollinearity, which is responsible for several interesting magnetic properties, such as weak ferromagnetism,[5] which has recently also been observed in SCMs.[6] In SMMs, spin noncollinearity has been associated with the generation of high-order terms in the magnetic anisotropy, which are mostly responsible for tunneling of the magnetization.[7] More recently, spin noncollinearity has been observed in a triangular dysprosium(III) cluster[8] and indeed predicted theoretically,[9] giving rise to spin chirality and slow magnetic relaxation together with a nonmagnetic ground state.

Anisotropic lanthanide ions are attracting increasing interest in molecular magnetism,[10] where they are often combined with 3d metal ions[11] or other magnetic centers.[12,13] Adequate analysis of the magnetic properties is in most cases lacking because of its complexity, thus hampering the development of a rational and efficient strategy to increase T_B in these systems. In fact,

[†] University of Florence.
[‡] INSA-Rennes.
[§] Universität Stuttgart.

(1) Gatteschi, D.; Sessoli, R.; Villain, J. *Molecular Nanomagnets*; Oxford University Press: Oxford, U.K., 2006.
(2) (a) Coulon, C.; Miyasaka, H.; Clérac, R. *Struct. Bonding (Berlin)* **2006**, *122*, 163. (b) Bogani, L.; Vindigni, A.; Sessoli, R.; Gatteschi, D. *J. Mater. Chem.* **2008**, *18*, 4750.
(3) Ako, A. M.; Hewitt, I. J.; Mereacre, V.; Clerac, R.; Wernsdorfer, W.; Anson, C. E.; Powell, A. K. *Angew. Chem., Int. Ed.* **2006**, *45*, 4926.
(4) Milios, C. J.; Vinslava, A.; Wernsdorfer, W.; Moggach, S.; Parsons, S.; Perlepes, S. P.; Christou, G.; Brechin, E. K. *J. Am. Chem. Soc.* **2007**, *129*, 2754.
(5) Morrish, A. H. *The Physical Principles of Magnetism*; John Wiley & Sons, Inc.: New York, 1966.
(6) (a) Bernot, K.; Luzon, J.; Sessoli, R.; Vindigni, A.; Thion, J.; Richeter, S.; Leclercq, D.; Larionova, J.; Van Der Lee, A. *J. Am. Chem. Soc.* **2008**, *130*, 1619. (b) Palii, A. V.; Ostrovsky, S. M.; Klokishner, S. I.; Reu, O. S.; Sun, Z. M.; Prosvirin, A. V.; Zhao, H. H.; Mao, J. G.; Dunbar, K. R. *J. Phys. Chem. A* **2006**, *110*, 14003.
(7) Barra, A. L.; Caneschi, A.; Cornia, A.; Gatteschi, D.; Gorini, L.; Heiniger, L. P.; Sessoli, R.; Sorace, L. *J. Am. Chem. Soc.* **2007**, *129*, 10754.
(8) (a) Tang, J. K.; Hewitt, I.; Madhu, N. T.; Chastanet, G.; Wernsdorfer, W.; Anson, C. E.; Benelli, C.; Sessoli, R.; Powell, A. K. *Angew. Chem., Int. Ed.* **2006**, *45*, 1729. (b) Luzon, J.; Bernot, K.; Hewitt, I. J.; Anson, C. E.; Powell, A. K.; Sessoli, R. *Phys. Rev. Lett.* **2008**, *100*, 247205.
(9) Chibotaru, L. F.; Ungur, L.; Soncini, A. *Angew. Chem., Int. Ed.* **2008**, *47*, 4126.
(10) (a) Ishikawa, N.; Sugita, M.; Ishikawa, T.; Koshihara, S.; Kaizu, Y. *J. Am. Chem. Soc.* **2003**, *125*, 8694. (b) Takamatsu, S.; Ishikawa, T.; Koshihara, S.; Ishikawa, N. *Inorg. Chem.* **2007**, *46*, 7250. (c) Aldamen, M. A.; Clemente-Juan, J. M.; Coronado, E.; Marti-Gastaldo, C.; Gaita-Arino, A. *J. Am. Chem. Soc.* **2008**, *130*, 8874. (d) Gamer, M. T.; Lan, Y.; Roesky, P. W.; Powell, A. K.; Clerac, R. *Inorg. Chem.* **2008**, *47*, 6581. (e) Westin, L. G.; Kritikos, M.; Caneschi, A. *Chem. Commun.* **2003**, 1012.

in low-symmetry environments, crystal-field analysis is not fully reliable because of the large number of parameters that must be included in the treatment. Ab initio post-Hartree−Fock calculations have recently been employed successfully to determine the magnetic anisotropy of a triangular Dy_3 cluster, but only an indirect comparison of the theoretical prediction with the single-ion anisotropy was possible.[9]

Here we combine theoretical and experimental investigations of a model exchange-coupled system comprising a Dy^{III} ion and organic radicals to shed light on the magnetic anisotropy and exchange interactions involving this otherwise intractable lanthanide ion. The interest in this type of system is many-sided. In fact, compounds comprising nitronyl nitroxide (NIT−R) radicals (NIT−R = 2-R-4,4,5,5-tetramethylimidazolidine-3-oxide-1-oxyl) and rare earths give rise to a multitude of interesting phenomena, including (*i*) relatively high temperature transitions to three-dimensional ferromagnetic order,[14] (*ii*) SMMs,[12,13] (*iii*) SCMs,[15] and (*iv*) chiral magnetic phases.[16] This last point is associated with the ability of rare earths, both diamagnetic and paramagnetic, to transmit relatively strong next-nearest-neighbor (NNN) exchange interactions between NIT−R radicals,[17] giving rise to spin frustration. The need to include NNNs in the analysis of the interactions inside exchange-coupled clusters is a general one, and it is very important to establish structural magnetic correlations in order to properly handle complex systems.[18]

We recently reported the synthesis and magnetic analysis of a family of 4f-based SCMs,[15] of which the Dy derivative having the formula $[Dy(hfac)_3(NIT-C_6H_4OPh)]_\infty$ (**1**) was the most deeply characterized.[15,19] Nevertheless, no analysis of the magnetic anisotropy of the rare earths could be provided, since simulation of the magnetic behavior of rare-earth-containing compounds is rather tricky. In fact, the spin-Hamiltonian approach, which works well for transition-metal ions, is less appropriate for rare earths because of the unquenched orbital momentum, and crystal-field analysis suffers from overparametrization problems. In the absence of detailed knowledge of the local magnetic anisotropy, no clear evidence of NNN interactions mediated by the anisotropic rare earth can in fact be detected through a simple analysis of the magnetic behavior.

In order to obtain information on complex systems, single-crystal EPR measurements allow for a full characterization of the magnetic anisotropy in compounds based on transition metals,[20] and a report is available on a cerium−iron derivative.[21] Unfortunately, most Dy^{III} derivatives, as well as $[Dy(hfac)_3(NIT-C_6H_4OPh)_2]$ (**2**), the monomeric analogue of **1**, are EPR-silent, since anisotropic rare earths present very fast electronic relaxation that broadens the EPR signal, hampering a precise determination of the **g** tensor.

Single-crystal magnetic measurements can provide information on the magnetic anisotropy through angle-resolved magnetometry. This technique was developed in the 1960s and has been used in the past to characterize the magnetic anisotropies of a huge variety of samples, mainly thanks to the fiberglass torque method.[22] However, it has scarcely been employed in molecular magnetism because of its complex procedure and low sensitivity, a problem recently solved with the integration of sample rotators in SQUID magnetometers. Another problem that has been detrimental to its widespread use is that, in many cases, the observed magnetization is the crystal average of molecules that are structurally identical but oriented differently in the crystal. This occurs when the site symmetry of the magnetic molecules is lower than that of the space group. For instance, a problem like this occurs in widely spread monoclinic lattices when the molecule is in a general position or on an inversion center. Triclinic crystals do not suffer this drawback but are more difficult to handle.

Monomeric species having the general formula $[Dy(hfac)_3(NIT-R)_2]$, when suited to single-crystal magnetization measurements, can allow the determination of the local magnetic anisotropy of the Dy ions, thus affording valuable information about Dy-based magnetic materials and **1** in particular. Screening of the outcome of the reaction of $Dy(hfac)_3 \cdot 2H_2O$ with $NIT-C_6H_4OR'$ radicals revealed that with R′ = ethyl, crystal-

(11) (a) Zaleski, C. M.; Depperman, E. C.; Kampf, J. W.; Kirk, M. L.; Pecoraro, V. L. *Angew. Chem., Int. Ed.* **2004**, *43*, 3912. (b) Osa, S.; Kido, T.; Matsumoto, N.; Re, N.; Pochaba, A.; Mrozinski, J. *J. Am. Chem. Soc.* **2004**, *126*, 420. (c) Mishra, A.; Wernsdorfer, W.; Abboud, K. A.; Christou, G. *J. Am. Chem. Soc.* **2004**, *126*, 15648. (d) He, F.; Tong, M.-L.; Chen, X.-M. *Inorg. Chem.* **2005**, *44*, 8285. (e) Mishra, A.; Wernsdorfer, W.; Parsons, S.; Christou, G.; Brechin, E. K. *Chem. Commun.* **2005**, 2086. (f) Costes, J.-P.; Auchel, M.; Dahan, F.; Peyrou, V.; Shova, M.; Wernsdorfer, W. *Inorg. Chem.* **2006**, *45*, 1924. (g) Mori, F.; Nyui, T.; Ishida, T.; Nogami, T.; Choi, K.-Y.; Nojiri, H. *J. Am. Chem. Soc.* **2006**, *128*, 1440. (h) Aronica, C.; Pilet, G.; Chastanet, G.; Wernsdorfer, W.; Jacquot, J.-F.; Luneau, D. *Angew. Chem., Int. Ed.* **2006**, *45*, 4659. (i) Ferbinteanu, M.; Kajiwara, T.; Choi, K.-Y.; Nojiri, H.; Nakamoto, A.; Kojima, N.; Cimpoesu, F.; Fujimura, Y.; Takaishi, S.; Yamashita, M. *J. Am. Chem. Soc.* **2006**, *128*, 9008. (j) Mereacre, V. M.; Ako, A. M.; Clérac, R.; Wernsdorfer, W.; Filoti, G.; Bartolome, J.; Anson, C. E.; Powell, A. K. *J. Am. Chem. Soc.* **2007**, *129*, 9248. (k) Zaleski, C. M.; Kampf, J. W.; Mallah, T.; Kirk, M. L.; Pecoraro, V. L. *Inorg. Chem.* **2007**, *46*, 1954. (l) Mereacre, V.; Ako, A. M.; Clérac, R.; Wernsdorfer, W.; Hewitt, E. J.; Anson, C. E.; Powell, A. K. *Chem.−Eur. J.* **2008**, *14*, 3577. (m) Stamatatos, T. C.; Teat, S. J.; Wernsdorfer, W.; Christou, G. *Angew. Chem., Int. Ed.* **2009**, *48*, 521. (n) Chandrasekhar, V.; Pandian, B. M.; Azhakar, R.; Vittal, J. J.; Clérac, R. *Inorg. Chem.* **2009**, *48*, 521. (o) Novitchi, G.; Wernsdorfer, W.; Chibotaru, L. F.; Costes, J.-P.; Anson, C. E.; Powell, A. K. *Angew. Chem., Int. Ed.* **2009**, *48*, 1614.

(12) (a) Luneau, D.; Rey, P. *Coord. Chem. Rev.* **2005**, *249*, 2591. (b) Sutter, J.-P.; Kahn, M. L.; Golhen, S.; Ouahab, L.; Kahn, O. *Chem.−Eur. J.* **1998**, *4*, 571. (c) Caneschi, A.; Dei, A.; Gatteschi, D.; Sorace, L.; Vostrikova, K. *Angew. Chem., Int. Ed.* **2000**, *39*, 246. (d) Caneschi, A.; Dei, A.; Gatteschi, D.; Massa, C. A.; Pardi, L. A.; Poussereau, S.; Sorace, L. *Chem. Phys. Lett.* **2003**, *371*, 694.

(13) Poneti, G.; Bernot, K.; Bogani, L.; Caneschi, A.; Sessoli, R.; Wernsdorfer, W.; Gatteschi, D. *Chem. Commun.* **2007**, 1807.

(14) (a) Benelli, C.; Caneschi, A.; Gatteschi, D.; Sessoli, R. *Inorg. Chem.* **1993**, *32*, 4797. (b) Benelli, C.; Caneschi, A.; Gatteschi, D.; Sessoli, R. *Adv. Mater.* **1992**, *4*, 504.

(15) (a) Bogani, L.; Sangregorio, C.; Sessoli, R.; Gatteschi, D. *Angew. Chem., Int. Ed.* **2005**, *44*, 5817. (b) Bernot, K.; Bogani, L.; Caneschi, A.; Gatteschi, D.; Sessoli, R. *J. Am. Chem. Soc.* **2006**, *128*, 7947. (c) Bernot, K.; Bogani, L.; Sessoli, R.; Gatteschi, D. *Inorg. Chim. Acta* **2007**, *360*, 3807.

(16) (a) Bartolome, F.; Bartolome, J.; Benelli, C.; Caneschi, A.; Gatteschi, D.; Paulsen, C.; Pini, M. G.; Rettori, A.; Sessoli, R.; Volokitin, Y. *Phys. Rev. Lett.* **1996**, *77*, 382. (b) Cinti, F.; Rettori, A.; Barucci, M.; Olivieri, E.; Risegari, L.; Ventura, G.; Caneschi, A.; Gatteschi, D.; Rovai, D.; Pini, M. G.; Affronte, M.; Mariani, M.; Lascialfari, A. *J. Magn. Magn. Mater.* **2007**, *310*, 1460.

(17) Benelli, C.; Gatteschi, D. *Chem. Rev.* **2002**, *102*, 2369.

(18) de Graaf, C.; de P. R. Moreira, I.; Illas, F.; Iglesias, Ò.; Labarta, A. *Phys. Rev. B* **2002**, *66*, 014448.

(19) Bernot, K.; Luzon, J.; Bogani, L.; Caneschi, A.; Gatteschi, D.; Sessoli, R.; Vindigni, A.; Rettori, A.; Pini, M. G. *Phys. Rev. B*, in press. A preprint is available from the arXiv.org e-Print archive at http://arxiv.org/abs/0901.4409.

(20) (a) Bencini, A.; Gatteschi, D. *Transition Met. Chem.* **1982**, *8*, 1. (b) Pilbrow, J. R. *Transition Ion Electron Paramagnetic Resonance*; Oxford University Press: Oxford, U.K., 1990. (c) Caneschi, A.; Gatteschi, D.; Lalioti, N.; Sessoli, R.; Sorace, L.; Tangoulis, V.; Vindigni, A. *Chem.−Eur. J.* **2002**, *8*, 286.

(21) Sorace, L.; Sangregorio, C.; Figuerola, A.; Benelli, C.; Gatteschi, D. *Chem.−Eur. J.* **2009**, *15*, 1377.

(22) (a) Mitra, S. *Prog. Inorg. Chem.* **1977**, *22*, 309. (b) Gerloch, M.; Mackey, D. J. *J. Chem. Soc., Dalton Trans.* **1972**, *3*, 415.

lization occurs in the triclinic $P\bar{1}$ space group with only one Dy center in the asymmetric unit. We thus investigated $[Dy(hfac)_3(NIT-C_6H_4OEt)_2]$ (**3**) and measured the susceptibility tensor at various temperatures. We then succeeded in rationalizing the observed magnetic anisotropy with predictions from an ab initio calculation, demonstrating that this theoretical approach can be used to reliably predict the nature, strength, and orientation of the magnetic anisotropy of rare earths. This mixed experimental−theoretical approach opens exciting perspectives on a deep insight into the magnetism of rare earths and for the design of improved SMMs and SCMs based on lanthanide ions.

Experimental Section

General Procedures and Materials. All of the chemicals and solvents used were reagent-grade. The starting materials, $[Dy(hfac)_3\cdot 2H_2O]$ ($hfac^-$ = hexafluoroacetylacetonate), $[Y(hfac)_3\cdot 2H_2O]$, and NIT−C_6H_4OEt radical [NIT−C_6H_4OEt = 2-(4′-ethoxyphenyl)-4,4,5,5-tetramethylimidazolidine-3-oxide-1-oxyl], were prepared as previously described.[15,23]

Syntheses. The monomeric compound **3** was prepared by dissolving 0.025 mmol of $[Dy(hfac)_3\cdot 2H_2O]$ in boiling *n*-heptane (40 mL) under stirring. When the volume reached 10−12 mL, the stirring proceeded on a cold rotator, and at 75 °C, 0.1 mmol (32 mg) of radical was quickly added. After 24 h, blue square crystals of **3** suitable for X-ray diffraction were collected in 85% yield. The same procedure was used to produce the Y^{III} analogue $[Y(hfac)_3(NIT-C_6H_4OEt)_2]$ (**4**), with the only difference being the use of $[Y(hfac)_3\cdot 2H_2O]$ as a reactant. Anal. Calcd for $C_{45}H_{45}N_4O_{12}F_{18}Dy$: Dy, 12.14; C, 40.38; H, 3.39; N, 4.18. Found: Dy, 12.12; C, 40.34; H, 3.44; N, 4.21. Anal. Calcd for $C_{45}H_{45}N_4O_{12}F_{18}Y$: Y, 7.03; C, 42.73; H, 3.58; N, 4.43. Found: Y, 7.01; C, 42.72; H, 3.58; N, 4.42.

Crystallography. X-ray data were collected at 150 K with an Oxford Diffraction Xcalibur3 diffractometer using Mo Kα radiation ($\lambda = 0.71073$ Å). Data reduction was accomplished using CrysAlis RED p 171.29.2. Absorption correction was performed using both ABSGRAB and ABSPACK software included in the CrysAlis package.[24] The ABSGRAB correction allows for the determination of μ parameter. The structure was solved by direct methods, developed by successive difference Fourier syntheses, and refined by full-matrix least-squares on all F^2 data using SHELXL 97.[25] Hydrogen atoms were included in calculated positions and allowed to ride on their parent atoms.

Crystal data for **3** ($Dy_1C_{45}H_{45}N_4O_{12}F_{18}$, $M = 1338.35$ g mol^{-1}): dark-blue prism; triclinic space group $P\bar{1}$ (No. 2); $a = 12.259(5)$ Å, $b = 14.235(4)$ Å, $c = 17.560(1)$ Å, $\alpha = 98.111(2)°$, $\beta = 103.836(5)°$, $\gamma = 111.260(8)°$; $V = 2683.6(16)$ Å^3; $Z = 2$; $T = 150(2)$ K; $\rho = 1.656$ g cm^{-3}; $\mu = 1.516$ mm^{-1}; R1= 0.0669, wR2= 0.1667. A relatively large residual electronic density (6.85 e Å^{-3}) was observed on the difference map, even after the final cycle of the refinement. Since the position of this peak is not consistent with the presence of any chemical species, such as solvent molecules, it can reasonably be related to a truncation artifact (Gibbs effect), as often observed in molecules containing heavy atoms such as lanthanides. The assignation of this peak as a carbon atom produced unrealistic values of R1 (0.513) and GOF (6.888), strengthening the above interpretation. The supplementary crystallographic data for this paper are available in the Supporting Information as well as in Cambridge Crystallographic Data Centre (CDCC) entry CCDC 684694, which is available free of charge from the CCDC via www.ccdc.cam.ac.uk/data_request/cif.

Magnetic Measurements. The angle-dependent magnetic measurements were performed with a Cryogenic S600 SQUID magnetometer equipped with an automatic horizontal sample rotator. Single-crystal ac susceptibility was measured with a Quantum Design MPMS SQUID magnetometer. The magnetization curve was obtained with a Vibrating Sample Magnetometer (Oxford Instruments MAGLAB2000 platform).

A crystal of **3** (1.48 mg) was placed on its (001) face on a Teflon cube and attached with Apiezon N grease along one edge of the cube, with an estimated error of ±3°. Three orthogonal faces of the cube were then employed to fix the sample on the platelet of a Quantum Design horizontal sample rotator adapted to work in a Cryogenic S600 SQUID magnetometer. The angle dependence was investigated over an angular range of more than 180° in three consecutive rotations performed along the three orthogonal crystallographic axes **a**, **b′**, and **c***, where **c*** is defined as **a** × **b** and **b′** is orthogonal to **a** and **c***, defining a right-handed frame. The signal was corrected for the diamagnetic contribution of the Teflon cube, which, however, was fundamental for better control of the orthogonality of the three rotations. Measurements were performed in a magnetic field of 1 kOe to avoid a strong torque on the crystal.

The same crystal was then placed on a specially designed support to measure its magnetization when the field was applied along the previously determined easy and hard axes. The temperature dependence of the magnetization was measured with a Quantum Design SQUID magnetometer, while the field dependence was measured up to 120 kOe with an Oxford Instruments Vibrating Sample Magnetometer. In this case, only the easy axis was investigated because the application of a field larger than 40 kOe resulted in a torque sufficient to detach and break the crystal. Measurements on a powder sample were performed with the same instruments, grounding crystals in a pellet.

Ab Initio Calculations. The post-Hartree−Fock ab initio calculations were carried out using the MOLCAS 7.0 program.[26] In the multiconfigurational approach used, relativistic effects were treated in two steps, both based on the Douglas−Kroll Hamiltonian.[27] Scalar terms were included in the basis-set generation and used to determine spin-free wave functions and energies through the use of the complete active space self-consistent field (CASSCF) method. Next, spin−orbit coupling was treated with the restricted active space state interaction (RASSI-SO) method,[28] which uses the CASSCF wave functions as the basis states. From the resulting eigenstates, the gyromagnetic tensor of the ground-doublet Kramers state was computed and diagonalized in order to obtain the three main anisotropy axes and the associated gyromagnetic values (g_x, g_y, and g_z).[29]

Results

Synthesis and Crystal Structure. Reaction of NIT−R radicals with $Dy(hfac)_3\cdot 2H_2O$ salts has previously been employed to obtain both chain compounds and various monomeric species,[13−15,17,30] depending on the stoichiometry of the reagents and the presence of water. The $Dy(NIT-R)_2$ stoichiometry was chosen to mimic the coordination around Dy^{III} in the chain compound. Additionally, it also allows information on the radical−radical NNN

(23) Ullmann, E. F.; Osiecki, J. H.; Boocock, D. G. B.; Darcy, R. *J. Am. Chem. Soc.* **1972**, *94*, 7049.
(24) *CrysAlis CCD and CrysAlis RED*, version 1.171.32.15; Oxford Diffraction Ltd.: Abingdon, U.K., 2008.
(25) Sheldrick, G. M. *SHELX-97: An Integrated System for Solving and Refining Crystal Structures From Diffraction Data*; University of Göttingen: Göttingen, Germany, 1997.
(26) Karlstrom, G.; Lindh, R.; Målmqvist, P. A.; Roos, B. O.; Ryde, U.; Veryazov, V.; Widmark, P. O.; Cossi, M.; Schimmelpfennig, B.; Neogrady, P.; Seijo, L. *Comput. Mater. Sci.* **2003**, *28*, 222.
(27) Hess, B. A.; Marian, C. M.; Wahlgren, U.; Gropen, O. *Chem. Phys. Lett.* **1996**, *251*, 365.
(28) Målmqvist, P. A.; Roos, B. O.; Schimmelpfennig, B. *Chem. Phys. Lett.* **2002**, *357*, 230.
(29) Vancoille, S.; Målmqvist, P. A.; Pierlot, K. *ChemPhysChem* **2007**, *8*, 1803.
(30) Lescop, C.; Belorizky, E.; Luneau, D.; Rey, P. *Inorg. Chem.* **2002**, *41*, 3375.

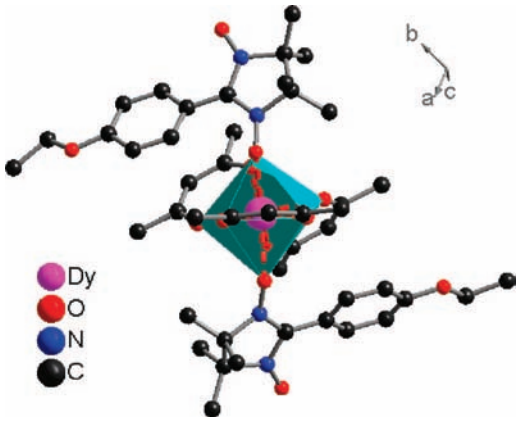

Figure 1. Representation of **3**, as seen from the idealized C_2 molecular symmetry axis. The coordination environment of the Dy^{III} ion is highlighted by the azure polyhedron. Fluorine and hydrogen atoms have been omitted for clarity.

interactions to be gathered. The mononuclear compound **2**, which is similar to a monomeric unit of **1**, crystallizes in a monoclinic space group with the metal ion in a general position. Consequently, it is not suited for angle-resolved magnetic measurements, as angle-resolved magnetometry provides the *crystal* magnetic susceptibility tensor, which corresponds to the *molecular* one only when the molecule has the same point symmetry as the crystal space group. However, a quantitative determination of the molecular χ tensor is possible for the triclinic system.[31] A screening of the outcomes of the reactions of $Dy(hfac)_3 \cdot 2H_2O$ with $NIT-C_6H_4OR'$ radicals revealed that compound **3** crystallizes in the triclinic $P\bar{1}$ space group with only one Dy center in the asymmetric unit. In **3**, the Dy ion is octacoordinated by three $hfac^-$ ligands and two oxygens belonging to the NIT−R radicals, as shown in Figure 1. The coordination polyhedron of each Ln^{III} ion is quite regular, with six $Dy-O_{hfac}$ distances ranging from 2.333(4) to 2.371(3) Å and two almost identical $Dy-O_{rad}$ distances of 2.328(3) and 2.331(3) Å. Selected bond distances and angles are listed in Table S2 in the Supporting Information.

The coordination geometries of the Dy ions in **1** and **3** are very similar to each other, with the highest discrepancies being 0.055 Å in the Dy−O bond length and 4.2° in the bond angle. The Supporting Information gives selected bond distances and angles (Table S2) and a superposition of the coordination polyhedra of **1** and **3** (Figure S3), which can be schematized as distorted square antiprisms.[32] This similarity is mainly due to the fact that despite the stoichiometry change, the same stacking interactions take place between the aromatic rings of the radicals and two of the three $hfac^-$ ligands, governing the geometrical arrangement of the complex. Consequently, as for **1**, the two radicals of **3** point in almost opposite directions.

The monomers are well-isolated one from another, with a minimum Dy−Dy distance of 10.06 Å. Neither intermolecular contacts through the noncoordinated NO groups of the radicals (minimum distance 4.26 Å) nor hydrogen bonds that could be responsible for intermolecular magnetic interactions are observed in the system. A representation of the crystal packing in **3** is provided in Figure S4 in the Supporting Information.

Magnetic Measurements. The angular dependence of the *M*/*H* ratio was measured in a static field of 1 kOe. At this field, the magnetization is almost linear in *H*, and the *M*/*H* ratio can be assumed to correspond to the susceptibility. Figure 2 shows that the susceptibility is highly dependent on the angle, particularly for the rotation around **b′**, where values span the range from 0.74 to 12.9 emu mol^{-1}.

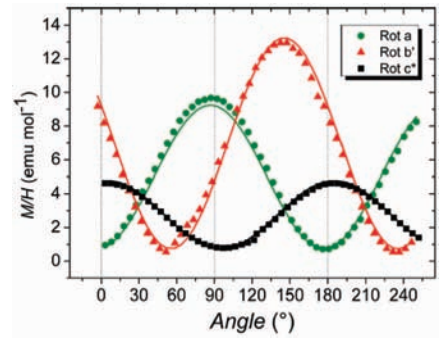

Figure 2. Angular variation of the molar susceptibility (*M*/*H* ratio) of **3** at $T = 2.5$ K along the three axes of the laboratory frame. At $\theta = 0$ and 90°, respectively, **H** is parallel to **b′** and **c*** for the rotation around **a**, **c*** and **a** for the **b′** rotation, and **a** and **b′** for **c*** rotation.

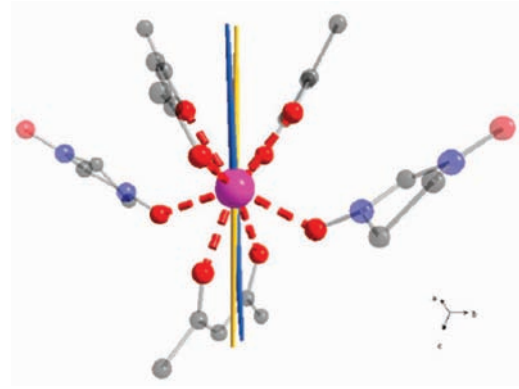

Figure 3. Representation of a molecule of **3** together with the easy axis as determined from the angular dependence of the susceptibility (yellow) and ab initio calculations (blue). The angle formed by the two directions is ~7°.

Similar to what is commonly done in single-crystal EPR analysis,[20] the data were fitted assuming the tensorial relation $\mathbf{M} = \chi\mathbf{H}$. For **H** rotating in the $\alpha\beta$ plane, we can use the expression

$$M(\theta) = \chi_{\alpha\alpha}H(\cos\theta)^2 + \chi_{\beta\beta}H(\sin\theta)^2 + 2\chi_{\alpha\beta}H\sin\theta\cos\theta \quad (1)$$

where α and β stand for the vectors **a**, **b′**, and **c*** in a cyclic permutation and θ is the angle between **H** and the α vector.

The best-fit procedure at $T = 2.5$ K (Figure 2) provided the full susceptibility tensor (see the Supporting Information), whose diagonalization afforded the three principal components $\chi_x = 0.2 \pm 0.1$, $\chi_y = 1.3 \pm 0.1$, and $\chi_z = 13.2 \pm 0.2$ emu mol^{-1}. The eigenvector matrix provides the molecular reference frame **x**, **y**, **z**, and the easy axis **z** is superimposed on the molecular structure in Figure 3 (the orientation of the three axes is shown in Figure S6 in the Supporting Information). The outcome of this analysis is a strong Ising-type magnetic anisotropy for **3**, with the easy axis along **z** and the hard and intermediate axes along **x** and **y**, respectively. The experimental data refer to a three-spin system, but the assumption that the anisotropy is determined by Dy^{III} appears to be a reasonable one. This result represents, to the best of our knowledge, the first direct

(31) De W. Horrocks, W., Jr.; De W. Hall, D. *Coord. Chem. Rev.* **1971**, *6*, 147.
(32) King, R. B. *J. Am. Chem. Soc.* **1969**, *91*, 7211.

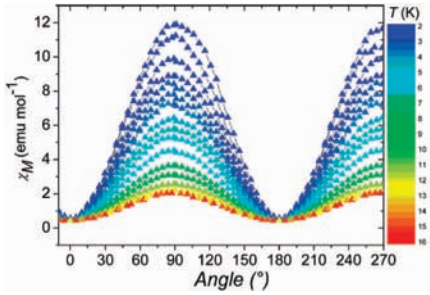

Figure 4. Angular variation of the susceptibility of **3** measured at different temperatures, as reported in the color scale, from 2 (blue) to 15 K (red). Rotations were performed around the **a** axis, and $\theta = 0$ and 90° correspond to measurements along **b′** and **c***, respectively.

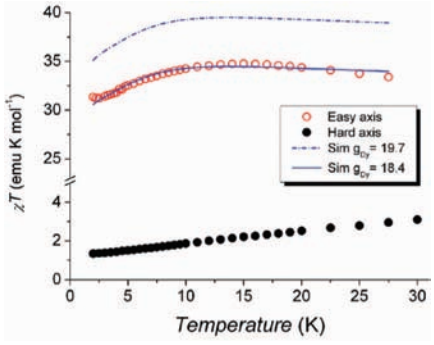

Figure 5. Temperature dependence of the χT product of **3** measured along the hard axis (black ●) and the easy axis (red ○). The lines are theoretical simulations based on an analytical expression derived from eq 2 using the parameter values $J_{NN} = -13.7$ cm^{-1}, $J_{NNN} = 15$ cm^{-1}, and either $g_{Dy} = 19.7$ (blue dash-dot curve) or $g_{Dy} = 18.4$ (blue solid curve), as reported in the Discussion.

estimation of the magnetic anisotropy of a rare-earth center in the absence of symmetry, and it shows that the easy axis lies not along any bond but rather through the approximate binary axis of the coordination environment (i.e., roughly the view axis of Figure 1).

Temperature-dependent measurements were then performed over the $T = 2-15$ K range at $H = 1$ kOe (see Figure 4 for the rotation along **a**). The χ values depend strongly on T, with a 10-fold reduction of the maximum values in going from 2 to 15 K, independent of the rotation axis. On the contrary, the minimum values remain roughly the same, and no shift of the positions of the extrema is observed.

Once angle-resolved magnetometry had provided the orientation of the easy axis, the temperature dependence of the magnetic susceptibility was measured along and perpendicular to it. The results, which are shown in Figure 5, confirm that the magnetic anisotropy remains constant up to 30 K. Over the investigated temperature range, the $\chi_z T$ product shows a rounded maximum at ~15 K that reaches a value of 34 emu K mol^{-1}.

By using the same sample holder, we also measured the H-dependence of M at $T = 1.6$ K for H up to 120 kOe (Figure 6). A plateau is observed between 10 and 60 kOe with a magnetization value of $\sim 10\mu_B$; beyond 70 kOe, M successively increases to reach a value of $11.8\mu_B$. With an increase in T, the jump is transformed into a linear increase in M. Measurements with the field perpendicular to the easy axis were not possible, as they resulted in a torque strong enough to break the crystal or detach it from the sample holder. However, it was possible to measure the magnetization of a powder sample with blocked microcrystals in a pellet. The corresponding magnetization

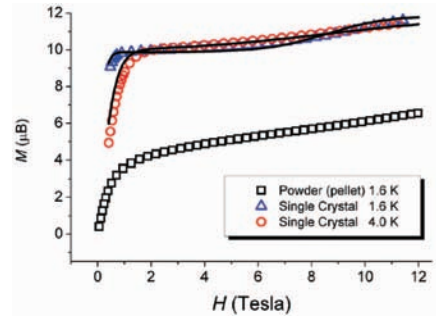

Figure 6. Field dependence of the magnetization of **3** measured on a single crystal with the field oriented along the easy axis at 1.6 (blue △) and 4 K (red ○) and on a powder pellet at 1.6 K (black □). The solid lines represent curves obtained using the analytical expression derived from the spin Hamiltonian (eq 2), as discussed in the text.

curve, which is also shown in Figure 6, differs significantly, being reduced by a factor of almost 2 and having no well-defined step even at low T.

Ab Initio Calculations. The low-lying energy levels of the Dy ion in the coordination environment of the X-ray structure were obtained via CASSCF calculations. A simplified molecular model was considered in order to reduce the otherwise too large computational time. The fluorides in the hfac$^-$ ligands were replaced by H atoms and the NITC_6H_4−OEt radicals by NIT−CH_3, and H atoms were added to the external oxygen atoms of the radicals, transforming them into closed-shell molecules in order to reduce the active space of the CASSCF calculations. In view of the internal nature of the 4f orbitals, they should be the most sensitive to ionic interactions, justifying the above assumptions.

All of the atoms were represented by basis sets of atomic natural orbitals from the ANO-RCC library, as implemented in the MOLCAS 7.0 quantum-chemistry package. The following contractions were used: [8s7p4d3f2g] for Dy; [3s2p] for O, C, and N; and [2s] for H. The CASSCF active space consisted of the Dy 4f orbitals, containing nine electrons in seven orbitals [CASSCF(9,7)]. CASSCF state average calculations of all of the sextets (21 roots) and all of the quadruplets (224 roots) were computed. As for the doublets, because of hardware limitations, a subset of 200 out of a total of 490 roots was considered in the state average calculations. With these CASSCF states, three different RASSI state interactions were computed in order to check the effect of the other energy levels on the spin−orbit splitting of the $^6H_{15/2}$ ground multiplet: first, a calculation (labeled as A in Table 1) including all of the multiplets having an energy gap of less than 40 000 cm^{-1} with respect to the $^6H_{15/2}$ multiplet (the ^{6}H, ^{6}F, and ^{6}P sextets, 108 quadruplets, and 32 doublets); second, a calculation (B) considering only the three sextets (^{6}H, ^{6}F, and ^{6}P); and finally, a calculation (C) using only the ^{6}H multiplet. The computed energies of the split levels of the ground $^6H_{15/2}$ multiplet and the principal g values of the ground Kramers doublet are listed in Table 1. The energy pattern is basically the same in the three calculations, indicating a small mixture of the ^{6}H multiplet with the other ones due to the spin−orbit coupling. Therefore, we performed a last CASSCF/RASSI calculation (D) considering only the 11 roots of the ^{6}H multiplet in the CASSCF state average and using them for the RASSI-SO state interaction. The energies of the $^6H_{15/2}$ multiplet and the g values from this last calculation are also listed in Table 1.

The magnetization easy axis, corresponding to the direction of the largest g component obtained from the last RASSI-SO

Table 1. Energy Levels of the $^6H_{15/2}$ Multiplet and Principal Gyromagnetic Factors for the Ground Kramers Doublet State Computed for Dy^{III} in **3** Using the CASSCF−RASSI-SO ab Initio Method

	A[a]	B[b]	C[c]	D[d]
	Energy Levels (cm^{-1})			
E_1	30.2	30.3	29.9	40.4
E_2	62.1	63.0	62.6	75.0
E_3	66.6	67.4	67.4	79.1
E_4	99.6	101.5	101.5	111.4
E_5	114.7	116.0	115.8	128.9
E_6	215.9	220.6	221.0	237.8
E_7	372.8	380.2	380.0	411.1
	Principal g Values			
g_x	1.5	1.7	1.8	1.0
g_y	1.3	1.4	1.4	0.9
g_z	17.6	17.5	17.4	18.2

[a] Includes in the RASSI-SO calculation all of the CASSCF roots in the 0−40 000 cm^{-1} energy range. [b] Same as A, except that only the sextet roots are considered. [c] Considers only the ^6H roots from a CASSCF state average calculation with a total of 18 sextet roots. [d] Same as C, but using a CASSCF state average calculation with the 11 lowest sextet roots.

computation, is represented together with the experimental one in Figure 3. The angle between the ab initio-computed and experimental easy axes is only 7°. This result allows us not only to confirm the experimental determination of the single-ion anisotropy axis but also to support the use of the CASSCF/RASSI-SO method as a suitable technique for the determination of single-ion easy anisotropy axes in lanthanide-based molecules.

Discussion

The ab initio calculations suggest a strong Ising-type magnetic anisotropy of the Dy ion at low temperature. A first rationalization of the observed magnetic behavior can be given by considering that the $^6H_{15/2}$ ground electronic state of the Dy^{III} ion is characterized by $g_J = {}^4/_3$.[17,33] The crystal-field interaction removes the $(2J + 1)$ degeneracy, yielding eight Kramers doublets. In the Ising limit, the ground doublet can be reasonably approximated by $m_J = \pm{}^{15}/_2$, with the first excited doublet separated by ∼60 K. Therefore, the low-T data can be interpreted by taking into account only the ground Kramers doublet, which can be treated as having the effective values $S_{\text{eff}} = {}^1/_2$, $g_z^{\text{eff}} = (2)({}^{15}/_2)g_J = 20$, and $g_{x,y}^{\text{eff}} = 0$. These data are in good agreement with the data in column D of Table 1. With respect to the magnetization, the M value observed at the plateau, $9.9\mu_B$, is very close to the value of $10\mu_B$ expected for this limiting case. The estimated g values compare well with those obtained by fitting the susceptibility data of Dy−NIT−R square dimers[13] and those reported in the literature that have been extracted from Mössbauer experiments[34] and other techniques.[33,35,36]

The observed magnetic behavior also suggests that the radicals are antiferromagnetically coupled and do not contribute significantly to M at low H. The increase in M at high H to reach the $11.92\mu_B$ value confirms the presence of an NNN antiferromagnetic interaction (J_{NNN}) between the radicals, which is broken by the applied magnetic field at $H = 120$ kOe.

The ability to obtain single-crystal magnetic data with H applied along the easy axis of the Dy^{III} ion allows a much simpler analytical treatment to be performed. With the assumption that the two radicals interact isotropically between themselves via a J_{NNN} coupling while an Ising interaction (J_{NN}) occurs with the $S_{\text{eff}} = {}^1/_2$ spin of Dy^{III}, the spin Hamiltonian becomes

$$\hat{H} = J\hat{\mathbf{S}}_{R1}\cdot\hat{\mathbf{S}}_{R2} + J'(\hat{S}_{R1z} + \hat{S}_{R2z})\sigma + g_{R1z}\hat{S}_{R1z}\mu_B H_z + g_{R2z}\hat{S}_{R2z}\mu_B H_z + g_{Dy}\mu_B\sigma H_z \quad (2)$$

where $\sigma = \pm{}^1/_2$ because of the Ising nature of Dy^{III}. The splittings of the four Kramers doublets present at zero magnetic field are then given by

$$E_{1,2} = \pm\frac{1}{2}g_{Dy}\mu_B H$$

$$E_{3,4} = J_{\text{NNN}} + \frac{1}{2}J_{\text{NN}} \pm (g_R + \frac{1}{2}g_{Dy})\mu_B H$$

$$E_{5,6} = J_{\text{NNN}} \pm \frac{1}{2}g_{Dy}\mu_B H$$

$$E_{7,8} = J_{\text{NNN}} - \frac{1}{2}J_{\text{NN}} \pm (g_R - \frac{1}{2}g_{Dy})\mu_B H$$

From these expressions, an analytical formula to reproduce the field and temperature dependence of the magnetization along the easy axis can easily be derived. Qualitative agreement with the experimental data is found for antiferromagnetic J_{NNN} and ferromagnetic J_{NN} values, with a sign alternation reminiscent of that observed for Gd-based compounds containing NIT−R radicals.[37] In this case, the $E_{1,2}$ doublet lies lowest for zero and weak applied fields. At a field $H_{co} = (J_{\text{NNN}} + {}^1/_2\, J_{\text{NN}})/(g_R\mu_B)$, a crossover with the first excited doublet $E_{3,4}$ occurs. As far as the level crossing is concerned, the two coupling constants J_{NNN} and J_{NN} are therefore strongly correlated to one another, and many sets of J_{NNN} and J_{NN} values reproduce the observed step. To solve this point, we synthesized $[Y(hfac)_3(NIT{-}C_6H_4OEt)_2]$ (**4**), which is structurally identical to **3** except for the substitution of Dy^{III} with the diamagnetic Y^{III} center. Analysis of the temperature dependence of the susceptibility of **4** with a Bleaney−Bowers formula (see the Supporting Information) affords a J_{NNN} value of 15(1) cm^{-1}. When this J_{NNN} magnitude is used for **3**, the best-fit values $g_{Dy} = 19.7(3)$ and $J_{\text{NN}} = -13.5(7)$ cm^{-1} for the Dy−radical interaction are found. Such a large value for the Dy−radical coupling constant J_{NN} is a direct consequence of using $S_{\text{eff}} = {}^1/_2$ for Dy^{III} but indeed corresponds to an exchange energy comparable to that observed for Gd^{III}−NIT−R derivatives.[38]

Despite the excellent agreement between the shapes of the simulated and experimental curves reported in Figure 6, the simulated ones show a more drastic jump of the magnetization near H_{co} and a flatter signal in the initial part of the plateau than do the experimental ones. Moreover, the simulation of the T dependence of χT along the single-ion easy axis using the

(33) Abragam, A.; Bleaney, B. *Electron Paramagnetic Resonance of Transition Ions*; Dover: New York, 1986.
(34) (a) Wickman, H. H.; Nowik, I. *Phys. Rev.* **1966**, *142*, 115. (b) Nowik, I.; Wickman, H. H. *Phys. Rev.* **1965**, *140*, 869. (c) Ofer, S.; Rakavy, M.; Segal, E.; Khurgin, B. *Phys. Rev.* **1965**, *138*, 241.
(35) (a) Bramwell, S. T.; Harris, M. J. *J. Phys.: Condens. Matter* **1998**, *10*, L215. (b) Flood, D. J. *J. Appl. Phys.* **1974**, *45*, 404. (c) Blote, H. W.; Wielinga, R. F.; Huiskamp, W. J. *Physica (Amsterdam)* **1969**, *43*, 549. (d) Janaa, Y. M.; Sengupta, A.; Ghosh, D. *J. Magn. Magn. Mater.* **2002**, *248*, 7.
(36) (a) Borowiec, M. T.; Dyakonov, V.; Prokhorov, A.; Szymczak, H. *Phys. Rev. B* **2000**, *62*, 5834. (b) Carlin, R. D. L. *Magnetochemistry*; Springer-Verlag: Berlin, 1986. (c) Bellesis, G. H.; Simizu, S.; Friedberg, S. A. *J. Appl. Phys.* **1987**, *61*, 3286.
(37) Benelli, C.; Caneschi, A.; Gatteschi, D.; Laugier, J.; Rey, P. *Angew. Chem., Int. Ed.* **1987**, *26*, 913.
(38) Benelli, C.; Caneschi, A.; Gatteschi, D.; Pardi, L.; Rey, P. *Inorg. Chem.* **1989**, *28*, 275.

previous best-fit parameters shows good qualitative agreement with experimental data, confirming that the J_{NNN} and J_{NN} values are correctly estimated; however, for quantitative agreement, the simulation requires a slightly reduced g_{Dy} value of 18.4, which is indeed closer to the value estimated from the ab initio calculations

The origin of the differences between the simulated and experimental data, in particular the discrepancy between the g values estimated from the high and low magnetic field experiments, can be envisaged by considering that CASSCF/RASSI-SO calculations suggest a relatively small separation between the ground and excited states inside the $^6H_{15/2}$ multiplet. The g_z value, in fact, does not approach the limiting value of 20 expected for a ground doublet corresponding to the pure $m_J = \pm^{15}/_2$ value, contrary to what is observed for the Dy_3 cluster.[11,12] In the case of **3**, as the ground Kramer's doublet is not an eigenstate of $\hat{J}_z$, the Zeeman term of the Hamiltonian produces an admixture of the ground and excited states, resulting in a nonlinear dependence of its energy as a function of H. These nonlinear terms in the Zeeman effect would account for the discrepancies observed at low field in Figure 6, namely, the smoother increase of the experimental magnetization versus the faster saturation of the simulated curve and the slightly smaller g_{Dy} value necessary to reproduce the experimental T dependence of χT along the single-ion easy axis measured at the relatively low applied field of 1000 Oe.

Other possibly relevant factors that were not considered in the model are the effects of thermal population of the other $^6H_{15/2}$ Kramers doublets of the Dy^{III} ion and a more complicated magnetic interaction between the radicals than just an isotropic one, since this interaction is mediated by the anisotropic spin density of Dy^{III}. Of course, it cannot be excluded that the energy levels may be somewhat populated above 15 K, but there is no doubt that the strong magnetic anisotropy requires that the low-temperature behavior is dominated by the population of the most anisotropic state. The small upturn observed in χT at the lowest investigated temperature cannot be ascribed to the excited states but could be due to either intermolecular weak dipolar interactions or an artifact introduced by the torque exerted on a nonperfectly aligned crystal.

Conclusions

In conclusion, we have demonstrated the power of a mixed experimental−theoretical approach in the analysis of the magnetic anisotropy and exchange interactions in molecular magnetic materials having a low-symmetry environment around the anisotropic lanthanide ion. In particular, using angle-resolved single-crystal magnetometry, we have obtained the orientation of the principal axes of the magnetization of a model system comprising Dy^{III} and organic radicals. With this information, a clear analysis of the T and H dependence of M has been possible, even in the presence of a strong orbital contribution.

A ferromagnetic Dy−radical interaction has been evidenced, as has the presence of antiferromagnetic NNN interactions between the radicals that are mediated by the Dy^{III} ion, analogous to what has previously been observed for diamagnetic[39] Y^{III} and Eu^{III} or isotropic Gd^{III} magnetic centers.[38] The collected information is currently being employed to analyze the more complex behavior of the first rare-earth-based SCM, **1**,[15,19] and a successful rationalization can be obtained by also assuming NNN antiferromagnetic interactions between Dy^{III} ions and a resulting spin-canted structure similar to that observed in Mn^{III}−porphyrine SCMs.[6]

These conclusions agree well with ab initio calculations based on the self-consistent field theory, which therefore seem to be a precious tool capable of predicting the nature and orientation of the magnetic anisotropy of rare earths in low-symmetry environments.

These experimental and theoretical approaches for characterizing anisotropic building blocks, both of which are affordable at a laboratory scale, are expected to become more and more frequently employed in molecular magnetism whenever a low-symmetry environment is encountered. The extracted information is fundamental in the rational design and full exploitation of SMMs and SCMs based on rare earths.

Acknowledgment. This work was supported by the German DFG (SPP1137-Molekularer Magnetismus), the EC "Network of Excellence" MagMaNet and RTN QuEMolNa (MRTN-CT2003-504880), the EC's Seventh Framework Programme ([*FP7/2007-2013*] under Grant Agreement [PIEF-GA-2008-220498]), and the Italian MIUR (FIRB and PRIN grants). M.S. acknowledges MagMaNet for funding of a training period in Florence.

Supporting Information Available: ORTEP view and crystallographic parameters for **3**, selected bond lengths and angles for **1** and **3**, representations of the coordination polyhedra of **1** and **3** and the crystal packing of **3**, temperature dependence of the $\chi_M T$ product of a powder sample of **3**, experimental procedure for the single-crystal magnetic measurements, the full susceptibility tensor of **3**, a view of the anisotropy principal axes of **3**, and temperature dependence of the magnetic susceptibility of **4**. This material is available free of charge via the Internet at http://pubs.acs.org.

JA8100038

(39) Benelli, C.; Caneschi, A.; Gatteschi, D.; Pardi, L.; Rey, P. *Inorg. Chem.* **1989**, *28*, 3230.